Modeling L-Band Brightness Temperature at Dome C in Antarctica and Comparison With SMOS Observations

Marion Leduc-Leballeur, Ghislain Picard, Arnaud Mialon, Laurent Arnaud, Eric Lefebvre, Philippe Possenti, Yann Kerr

Modeling L-band brightness temperature at Dome C, Antarctica and comparison with SMOS observations

Marion Leduc–Leballeur, Ghislain Picard, Arnaud Mialon, Laurent Arnaud, Eric Lefebvre, Philippe Possenti and Yann Kerr

***Abstract*—Two electromagnetic models were used to simulate snow emission at L-band from in situ measurements of snow properties collected at Dome C in Antarctica. Two different approaches were used: one based on the radiative transfer theory, and the other on the wave approach. The Soil Moisture Ocean Salinity (SMOS) satellite observations performed at 1.4 GHz (21 cm) were used to check the validity of these models. Model results based on the wave approach were in good agreement with SMOS observations, particularly for incidence angles lower than 55°. Comparisons suggest that the wave approach is more suitable to simulate brightness temperature at L-band than the transfer radiative theory, because interference between the layers of the snowpack is better taken into account.**

The model based on the wave approach was then used to investigate several L-band characteristics at Dome C. The emission e-folding depth, i.e. 67% of the signal, was estimated at 250 m, and 99% of signal emanated from the top 900 m. L-band brightness temperature is only slightly affected by seasonal variations in surface temperature, confirming the high temporal stability of snow emission at low frequency. Sensitivity tests showed that a good knowledge of density variability in snowpack is essential for accurate simulations in L-band.

***Index Terms*—Microwave, Radiative transfer theory, Remote sensing, Snow, Wave theory.**

I. Introduction

REMOTE sensing observations are particularly important for the study of the Antarctic climate because in situ measurements are very sparse [1]. Remote sensing is a unique means to obtain a detailed picture of the spatial and temporal variations in important climate variables.

Microwave radiometers operating at high-frequency (6 GHz and above) provide a 3-decade time series of observations recorded almost every day and in all weather conditions. These observations are very sensitive to snow properties at depth because of the ability of microwaves to penetrate depths ranging from a few centimeters at 100 GHz to a few hundred meters at 1 GHz [2]. Many studies have been performed to estimate surface or subsurface temperatures (e.g. [2]–[4]). However, successful retrieval of the temperature of the snow from microwave data is difficult because it requires accurate estimation of snow emissivity. Indeed, at high frequencies, snow is usually far from a black body [5], i.e., snow emissivity is significantly less than unity due to volume scattering caused by the granular structure of the snow. Since this structure is highly variable in space and time in Antarctica, snow emissivity is difficult to estimate or predict with sufficient accuracy to retrieve temperature.

At low microwave frequencies, scattering is weak compared to absorption, and the emissivity is close to unity when the surface reflection vanishes, which is the case at vertical polarization near the Brewster angle ($\sim$50°). As a consequence, the spatial variations in emissivity at L-band should be lower and more predictable than at higher frequencies. In this context, both the European Space Agency's (ESA) Soil Moisture Ocean Salinity (SMOS) [6] and the National Aeronautics and Space Administration's (NASA) Aquarius mission [7] carrying space-borne sensors operating at the lowest frequency available (1.4 GHz, L-band), offer a new opportunity to provide useful information about firn temperature over Antarctica.

There is thus a need for a better understanding of the characteristics of microwave emission by snow at L-band in Antarctica. Here, we present an electromagnetic model to predict the snow emission at L-band from in situ measurements of snow properties collected at Dome C (75°S, 123°E) in Antarctica.

Several models are available to compute microwave emission from given snow properties and different approaches have been developed. The radiative transfer (RT) theory is widely used to compute the propagation of the energy flux through the snowpack, which is represented as a stack of horizontal layers with given homogeneous scattering and absorption coefficients. The different models using this theory, including Helsinki University of Technology model (HUT/TKK; [8]), Microwave Emission Model of Layered Snowpacks (MEMLS; [9]) and Dense-Medium Radiative Theory (DMRT; [10]), mainly differ in the relationship used to link snow properties to these coefficients. However, because they all rely on RT theory, only the propagation of the incoherent wave is explicitly taken into account and the interference phenomena are ignored. But, interferences within the layers are particularly important when the thickness of the layer is in the order of -or less than- that of the wavelength, which is more pronounced at L-band than at higher frequencies. Ad hoc correction can be used to account for such phenomena (e.g. "coherent" layers in MEMLS), but it is not the ideal solution when the layer is

M. Leduc–Leballeur, G. Picard, L. Arnaud, E. Lefebvre and P. Possenti are with the LGGE (CNRS, Univ. Grenoble Alpes), Grenoble, F-38041, France (e-mail: leduc-leballeur@ujf-grenoble.fr).

A. Mialon and Y. Kerr are with the CESBIO (CNES, CNRS, IRD, UPS), Univ. Toulouse, F-31401 Toulouse Cedex 09, France.

Manuscript received March 28, 2014; revised July 4, 2014; accepted December 7, 2014.

much less thick than the wavelength. An alternative to RT is to compute the emission and propagation of waves, instead of the energy flux to explicitly account for interference phenomena. This alternative is often called "coherent approach". As it is derived from Maxwell's equation, it requires considerable simplification of the medium description to be computationally realistic. Such approaches have been successfully used (e.g. [11], [12]).

The objective of this study was to select the most suitable method to simulate L-band microwave emission and to assess the sensitivity to snow properties. To this end, we compared the DMRT theory based model presented in Picard *et al.* [13] to a coherent model derived from West *et al.* [12]. These models were forced with measurements collected at Dome C in 2012–2013 specifically to conduct L-band investigations. These measurements are unique as they provide grain size and density at a 5-cm vertical resolution, thus making it possible to distinguish individual layers, and down to a depth of 80 m, particularly useful considering the large emission e-folding depth at low microwave frequencies.

In the following sections, we present microwave observations collected by SMOS, the models and the input data, after which we present our results including an evaluation of the models and a sensitivity analysis. In the last section, we draw some conclusions.

II. Microwave observations

The SMOS satellite consists of an L-band (1.4 GHz – 21 cm) 2-D interferometric radiometer with an averaged ground resolution of 43 km [14]. The satellite provides multi-angular fully polarized brightness temperatures [15]. Only the horizontal (H) and vertical (V) polarizations were used in this study. The radiometric accuracy over snow is 3 K on average but depends on the angle of incidence (e.g. about 4 K at 0° and 2 K at 32.5°).

The SMOS Level 1C products contain multi-angular brightness temperatures at the top of the atmosphere in the antenna polarization reference frame. The product is geolocated in an equal-area grid system (ISEA 4H9V – Icosahedral Snyder Equal Area projection), with an oversampled resolution of about 15 km [15]. The reprocessed L1C product version 601 was used for this study. L1C brightness temperature was projected from the antenna reference frame to the Earth's surface reference frame and corrected for Faraday rotation using an algorithm provided by the CESBIO team (http://www.cesbio.ups-tlse.fr/SMOS_blog/wp-content/uploads/TOOLS/XY2HV.m).

To explore the Dome C area, time series acquired at the nearest grid point (75°07.7'S, 123°25.2'E) from March 2010 to February 2013 were extracted. The surrounding cells show very similar data [16]. In addition, the signal is very stable over the period, i.e. temporal variations are within the instrument noise range. Thus, in the following, only time-averaged data over the entire period are considered. The average is calculated over each 5° step of incidence angles from 0° to 65°. From about 1000 samples (at 0° and 65°) to 8000 samples (at 40°) are included for each step, which provides precision at an average of 4.8 K.

L-band brightness temperatures from ESA DOMECair experiment in 2013 [17] are used to check spatial variability inside the SMOS pixel. The standard deviation of observations was less than 1 K suggesting that the L-band signature over SMOS field of view in this area was relatively homogeneous. Occasional strong variations (∼5 K) can be observed in DOMECair data, but it seems to correspond to very local peaks, not representative of the whole SMOS pixel.

Note that brightness temperatures in L-band are only very slightly affected by the atmospheric water vapor and gas constituents, all the more true in Antarctica, where the air is particularly dry and cold. Thus, these observations are comparable with simulations that only consider snow without extra contributions (effects of the atmosphere, galactic noise, etc).

III. Electromagnetic modeling

A. Incoherent model

The incoherent model used is DMRT-ML (Dense Media Radiative Transfer - MultiLayer [13], available from http://lgge.osug.fr/∼picard/dmrtml/). It is based on the DMRT theory [18]. This model was primarily developed for microwave frequencies higher than L-band. It was used at Dome C with in-situ snow measurements as inputs and compared to satellite observations at 18.7 and 36.5 GHz [19] or ground-based observations at 11, 19 and 37 GHz [13]. It was also used in Antarctica to retrieve snow properties from 18.7 and 36.5 GHz observations [19].

The model describes the snowpack as a multi-layer medium, where each snow layer is characterized by its thickness, temperature, density, grain size, stickiness parameter and liquid water content. In this study, stickiness is not investigated because scattering by grains is negligible and this parameter has no effect in L-band (typically less than 0.1 K). The liquid water content of dry snow is considered to be zero. For each layer, the effective dielectric constant is solved using the first-order quasi-crystalline approximation and the Percus-Yevik approximation for non-sticky grains, i.e. grains without aggregates [18].

DMRT-ML can be applied to snow or firn. Snow is described as ice spheres in an air background while firn is described as air bubbles included in ice [20]. The absorption and scattering coefficients are calculated assuming a medium of "ice spheres in air" for densities lower than half that of the pure ice density (∼458.5 kg m^{-3}) and "air spheres in ice" otherwise [13].

The emission and propagation of radiation through the snowpack are computed using the Discrete Ordinate Method (DISORT; [21]), which takes multiple scattering between the layers into account. 32 streams are used here.

B. Coherent model

The coherent model is based on West *et al.* [12]. The derivation is also presented in Tsang *et al.* [22]. The medium is multi-layered and each layer is characterized by thickness, temperature and density. The most important simplification in this model is to neglect scattering by snow grains. This

assumption is invalid for high frequencies. However, at low frequencies (<∼10 GHz), since the wavelength is several orders of magnitude larger than grain size, scattering by grains is insignificant in comparison with absorption and scattering caused by the reflections at the interfaces between layers [23].

Under these assumptions, the vertically and horizontally polarized brightness temperatures of a given snowpack is calculated with the propagation-matrix formulation from Tsang *et al.* [24] for a single incidence angle θ_0:

$$\begin{aligned} T_{Bh}(\theta_0) = & \frac{k}{\cos\theta_0}\frac{\varepsilon_t'' T_t}{2\varepsilon_0 k_{tz}''}\left|B_t\right|^2 e^{-2k_{tz}'' d_n} \\ & + \frac{k}{\cos\theta_0}\sum_{l=1}^{n}\frac{\varepsilon'' T_l}{2\varepsilon_0}\left\{\frac{\left|A_l\right|^2}{k_{lz}''}(e^{2k_{lz}'' d_l} - e^{2k_{lz}'' d_{l-1}})\right. \\ & - \frac{\left|B_l\right|^2}{k_{lz}''}(e^{-2k_{lz}'' d_l} - e^{-2k_{lz}'' d_{l-1}}) \\ & + \frac{iA_l B_l^*}{k_{lz}'}(e^{-i2k_{lz}' d_l} - e^{-i2k_{lz}' d_{l-1}}) \\ & \left. - \frac{iA_l^* B_l}{k_{lz}'}(e^{i2k_{lz}' d_l} - e^{i2k_{lz}' d_{l-1}})\right\} \end{aligned} \quad (1)$$

$$\begin{aligned} T_{Bv}(\theta_0) = & \frac{k}{\cos\theta_0}\frac{\varepsilon_t'' T_t(\left|k_{tz}\right|^2 + k_x^2)}{2\varepsilon_0 k_{tz}'' \left|k_t\right|^2}\left|D_t\right|^2 e^{-2k_{tz}'' d_n} \\ & + \frac{k}{\cos\theta_0}\sum_{l=1}^{n}\frac{\varepsilon'' T_l(\left|k_{lz}\right|^2 + k_x^2)}{2\varepsilon_0 \left|k_l\right|^2} \\ & \times \left\{\frac{\left|C_l\right|^2}{k_{lz}''}(e^{2k_{lz}'' d_l} - e^{2k_{lz}'' d_{l-1}})\right. \\ & - \frac{\left|D_l\right|^2}{k_{lz}''}(e^{-2k_{lz}'' d_l} - e^{-2k_{lz}'' d_{l-1}}) \\ & + \frac{\left|k_{lz}\right|^2 - k_x^2 C_l D_l^*}{\left|k_{lz}\right|^2 + k_x^2 i k_{lz}'}(e^{-i2k_{lz}' d_l} - e^{-i2k_{lz}' d_{l-1}}) \\ & \left. - \frac{\left|k_{lz}\right|^2 - k_x^2 C_l^* D_l}{\left|k_{lz}\right|^2 k_x^2 i k_{lz}'}(e^{i2k_{lz}' d_l} - e^{i2k_{lz}' d_{l-1}})\right\} \end{aligned} \quad (2)$$

where the plane of observation is assumed the xz-plane, so $k_y = 0$; $k_l = k_l' + ik_l'' = \omega\sqrt{\epsilon_l \mu}$, with ϵ_l the permittivity of layer l and μ the permeability; $k_x = k_0 \sin\theta_0$ is real and constant throughout the stratified medium; $k_{lz} = \sqrt{k_l^2 - k_x^2}$; d_l is the depth of layer; the last layer with index t is semi-infinite and is at a depth of d_n; the constants A_l, B_l, C_l and D_l are the amplitudes of the waves, determined by recurrence relation:

$$\begin{aligned} \frac{A_l}{B_l}e^{-i2k_{lz}d_l} = & \frac{\frac{A_{(l+1)}}{B_{(l+1)}}e^{-i2k_{(l+1)z}d_{(l+1)}}}{\frac{A_{(l+1)}}{B_{(l+1)}}e^{-i2k_{(l+1)z}d_{(l+1)}}} \\ & \times \frac{e^{2ik_{(l+1)z}(d_{(l+1)} - d_l)} + R_{l(l+1)h}}{R_{l(l+1)h}e^{2ik_{(l+1)z}(d_{(l+1)} - d_l)} + 1} \end{aligned} \quad (3)$$

where $R_{l(l+1)h}$ is the Fresnel reflection coefficient for H polarization between layers l and $l+1$:

$$R_{l(l+1)h} = \frac{\mu_{(l+1)}k_{lz} - \mu_l k_{(l+1)z}}{\mu_{(l+1)}k_{lz} + \mu_l k_{(l+1)z}} \quad (4)$$

C_l and D_l satisfy the same recurrence relation as A_l and B_l, except that $R_{l(l+1)h}$ is replaced by $R_{l(l+1)v}$, the vertically polarized Fresnel reflection coefficient. $R_{l(l+1)v}$ is obtained by replacing μ by ϵ in (4).

As is true of any model based on the wave approach, the result obtained for a specific snowpack configuration (i.e. a given set of inputs) may differ considerably from those obtained with a slightly different snowpack, which is not the case with the RT approach, as this is less sensitive to snowpack variations. This is due to the high sensitivity of interference phenomena to layer optical depth. To account for the variable nature of the snowpack at the scale of a pixel (i.e. ∼43 km wide for SMOS), it is essential to average a large number of simulations using inputs that represent natural variability. As thousands of simulations are required, it would be impossible to obtain the input profiles from direct measurements. The procedure used to generate such profiles from measurements is based on West *et al.* [12] and is described in Section IV-B. The output of the model is the average of brightness temperatures over all the generated profiles.

The coherent model is hereafter called WALOMIS (Wave Approach for LOw-frequency MIcrowave emission in Snow).

C. Ice dielectric constant

The value of ice permittivity used in the models is critical at low frequencies. As a first approximation, emissivity can be simply described with scattering and absorption processes, scattering being driven by the contrast of the real part of permittivity between layers, and absorption by the imaginary part (also called dielectric loss). The emission e-folding depth mainly depends on absorption at low frequencies.

The real part of ice permittivity is usually well known and relatively constant over the microwave range. It has only a weak temperature dependence. In contrast, the imaginary part is difficult to measure at low frequencies due to its low magnitude (typically $\sim 10^{-3}$ at 1 GHz and -20°C [25]). It is difficult to define an accurate model to compute the imaginary part due to discrepancies among datasets derived from different experimental setup [26]–[28]. In this study, two empirical formulae were tested.

The first formula was deduced from measurements by Mätzler [23], [29] for microwave range (1-200 GHz):

$$\begin{aligned} \varepsilon_{iceM}'' &= \frac{\alpha}{\nu} + \beta\nu, \\ \alpha &= (0.00504 + 0.0062\theta)\exp(-22.1\theta), \\ \beta &= \frac{0.0207}{T}\frac{\exp(\frac{335}{T})}{(\exp(\frac{335}{T}) - 1)^2} + 1.16 \cdot 10^{-11}\nu^2 \\ &\quad + \exp(-9.963 + 0.0372(T - 273.16)), \\ \theta &= \frac{300}{T} - 1 \end{aligned} \quad (5)$$

where T is the temperature in Kelvin and ν is the frequency in GHz. This formulation is implemented in the original version of DMRT-ML [13].

The second formula comes from Tiuri *et al.* [25]. It is defined for frequencies from 840 MHz to 12 GHz:

$$\varepsilon''_{iceT} = 1.59 \cdot 10^6 \cdot (0.52\rho_i + 0.62\rho_i^2) \times (\nu^{-1} + 1.23 \cdot 10^{-14}\sqrt{\nu}) \exp(0.036(T - 273.16)) \quad (6)$$

where ρ_i = 0.917 g cm^{-3} is the ice density. It was recently used for C- and Ku-band studies (e.g. [30])

IV. Snow properties

A. In situ measurements profiles

The DMRT-ML and WALOMIS models require the thickness, temperature and density of each layer. In addition, DMRT-ML requires the grain size. The density profile is particularly important at L-band because it strongly controls the internal reflections and absorption that dominate the signal at low frequencies. For this reason, dedicated in situ measurements were carried out in Dome C area during the austral summer campaign 2012–2013 with a focus on long ice-core and high resolution measurements. Ten cores were extracted and processed for density and grain size measurements every 5 cm (Table I) representing a total of 4637 samples. These cores are 11 m to 30 m long and two are 80 m long, corresponding to the ice sheet part where the density is the most variable. It means that these measurements are representative enough of the relatively homogeneous SMOS pixel around Dome C (see Section II) to provide reliable comparison.

To perform objective density measurements on such a large number of samples, we developed a system at LGGE composed of a digital camera to quickly measure surface area and thickness of the samples and a balance to measure their mass. Note that measurements were not at regular intervals along the profiles, mainly due to the low cohesion of snow near the surface but also to technical problems. The number of samples per 2-m layer ranges from 37 to 30, depending on the layer. In addition, between 5 and 10 mm are inevitably lost for every sample at the time of cutting due to the saw blade thickness. The samples were consequently less than 5 cm thick. Fig. 1a shows the two 80-m long density profiles. Density was highly variable but follows an increasing trend with depth from about 350 kg m^{-3} at the surface to 800 kg m^{-3} at a depth of 80 m. In parallel, density variability decreased with depth, with a local minimum around a depth of 50 m. These characteristics are in agreement with other studies in Antarctica (e.g. [31]–[34]).

Grain size was measured with POSSSUM [35], an instrument based on the relationship between SWIR-reflectance and snow specific surface area (SSA), i.e. the total area of the air-snow interface per unit mass (m^2 kg^{-1}). Every sample was presented to POSSSUM in the cold laboratory at Concordia station. Snow grain size was deduced from measured SSA. First, SSA is converted into the optical radius using $r_{opt} = 3/(\rho_{ice} SSA)$ where ρ_{ice} = 917 kg m^{-3} is the pure ice density at 0°C [36]. Second, the optical radius must be scaled by an empirical factor ϕ to increase scattering by snow grains and obtain modeling results in reasonable agreement with observations at 18.7 and 36.5 GHz [19]. At Dome C, $\phi = 2.8$ [19]. The need to apply a ϕ factor was further confirmed but with slightly different values [37], [38]. Fig. 1b shows the grain size of two 80 m profiles. The snow grain size increased with depth from about 300 μm at the surface to 1000 μm at 80 m depth, in agreement with Durand *et al.* [39].

TABLE I
Cores extracted during 2012–2013 austral summer on Dome C

N°	Date	Location	Length	Samples
1	22/11/2012	75°06.2'S; 123°20.4'E	11.0 m	177
2	28/11/2012	75°06.0'S; 123°18.1'E	16.5 m	250
3	4-8/12/1012	75°05.7'S; 123°30.8'E	80.6 m	1442
4	10-11/12/2012	75°06.2'S; 123°20.2'E	30.1 m	499
5	15-19/12/2012	75°06.5'S; 123°21.7'E	80.0 m	1384
6	2/01/2013	75°19.3'S; 123°23.4'E	13.5 m	171
7	3/01/2013	74°52.8'S; 123°25.1'E	14.0 m	167
8	4/01/2013	75°09.2'S; 124°11.8'E	13.9 m	126
9	5/01/2013	75°06.5'S; 122°28.6'E	14.9 m	199
10	10/01/2013	75°04.7'S; 123°26.5'E	14.5 m	222

Snow temperature profiles were recorded at hourly intervals from December 2006 to December 2009, about 1 km to the west of Dome C. 35 probes were installed down to a depth of 21 m, with 14 probes in the top 2 m of the snowpack (at 0.1 m intervals to a depth of 0.6 m then at 0.2 m intervals down to 2 m). All the probes were inter-calibrated with a relative accuracy of $\pm$0.01 K and the absolute precision is $\pm$0.03 K [19]. For this study, monthly averaged temperature profiles were used. Fig. 1c shows mean profiles in January and July. In January, temperature decreased from -30°C at the surface to the minimum, -56°C, at 5 m, after which the temperature slightly increased to -55°C at 10 m. In comparison, in July the surface temperature was about 35°C colder but this difference quickly decreased to 10°C at 2 m and the temperature reaches -55°C at 10 m. In situ measurements performed to a depth of 3200 m at Dome C were used to complete the profiles and showed that below 10 m, temperature was almost constant at around -55°C down to 50 m and then decreased linearly to -3°C at a depth of 3200 m (see [40]).

Due to the large emission e-folding depth at L-band, it is essential to provide realistic snow characteristics down to the bedrock. Measured profiles were extrapolated down to 3200 m in depth, the thickness of the snowpack at this location [41]. DMRT-ML requires the radius of scatterers as input. For densities less than half that of pure ice, this corresponds to the radius of ice sphere while for higher densities, it corresponds to the air bubble radius. The values used were taken from the literature. Between 100 m and 1100 m in depth, the air bubble radius was linearly estimated from 180 μm to 50 μm [42], [43]. Due to increasing overburden pressure, the bubbles enclosed in ice shrink with depth until they become thermodynamically unstable and convert into air hydrates. Between 600 m and 1100 m, air bubbles and air hydrates coexist, and below this transition zone, the snowpack is considered to be air bubble free down to the bedrock [44], [45]. However, below 600 m, the air bubble radius is less than 100 μm. For this study, we chose to define a pure ice region

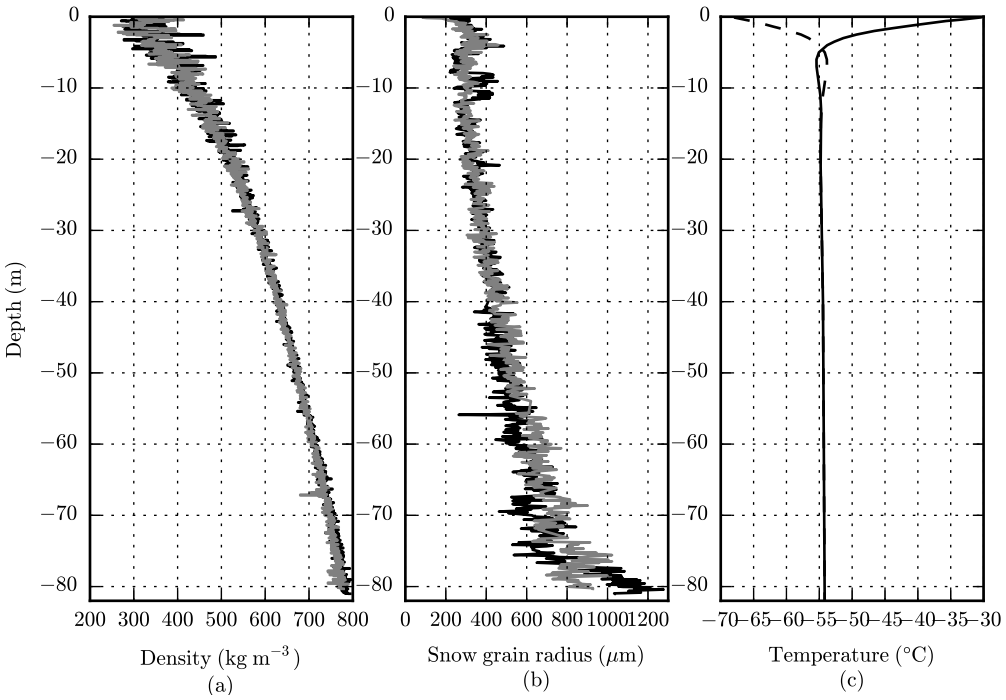

Fig. 1. (a) Snow density (kg m^{-3}) and (b) grain size (μm) profiles measured on two ice-cores at Dome C in the 2012–2013 austral summer; (c) Mean temperature profiles (°C) in January (solid line) and July (dashed line).

between 600 m and the bedrock as being air bubble free, where density reaches 922 kg m^{-3}. This value is in good agreement with measurements performed below 600 m in Antarctica at Vostok (78°S, 106°E; [44]) and Dome Fuji (77°S, 39°E; [46]). Density was linearly extrapolated from the last values measured at 80 m and 922 kg m^{-3} at 600 m.

To illustrate how temperature affects dielectric loss, Fig. 2 shows dielectric loss profiles calculated down to the bedrock using the density and temperature profiles and formulae described in the previous section. The ε''_{iceT} values are higher by about 0.2 10^{-3} than ε''_{iceM} values. Along the whole profile, ε''_{iceT} is more influenced by snow temperature than ε''_{iceM}. Indeed, at the surface, ε''_{iceT} decreases down to 5 m and then increases slightly down to 10 m, following the temperature profile (Fig. 1c). Below 100 m, where temperature increases with depth, ε''_{iceT} also increases. This results in a marked difference from ε''_{iceM}, which is almost constant along the snowpack.

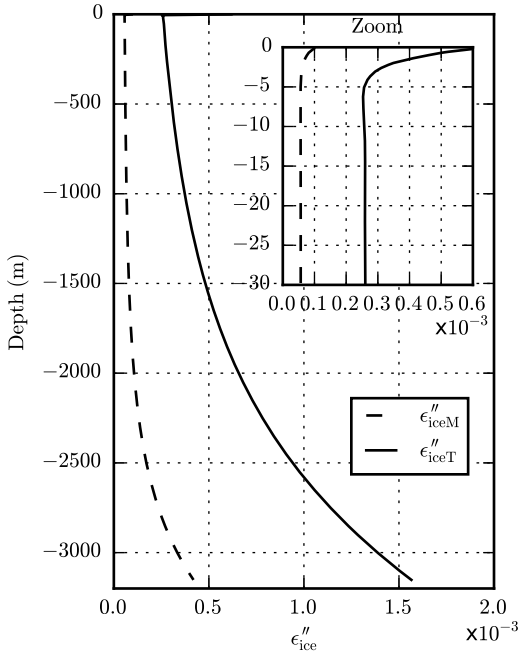

Fig. 2. Ice dielectric loss (ε''_{ice}) profile computed with Mätzler [29] (dashed line) and Tiuri *et al.* [25] (solid line).

B. Generation of stochastic snow density profiles

To generate the large number of density profiles required by WALOMIS to represent the natural variability within a SMOS pixel, we proceeded in two steps following West *et al.* [12]: i) to derive a statistical model from the measurements, and ii) to generate a large number of snow density profiles with similar statistical characteristics.

The measured density profiles were first decomposed into a smooth deterministic part $F(z)$ representing the general trend, and a zero mean random part $X(z)$ representing the variability around the trend: $D(z) = F(z) + X(z)$. $F(z)$ was obtained assuming an exponential form with unknown amplitude and decay. The two 80-m long profiles fitted in the least-squares sense with a imposed value of 922 kg m^{-3} below 600 m, matching the pure ice region defined in Section IV-A (Fig. 5a):

$$F(z) = 922 - 586\exp(0.017z) \quad (7)$$

where z is a negative value in meters. This fit is in agreement with empirical depth-dependent density relationship [47] and

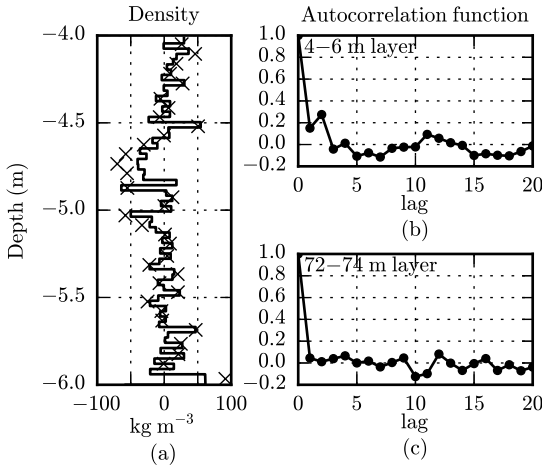

Fig. 3. (a) Measured (crosses) and re-sampled density profile 1 between 4 and 6 m deep at 3 cm resolution. Autocorrelation function (b) in the 4-6 m layer and (c) in the 72-74 m layer. One lag is 3 cm.

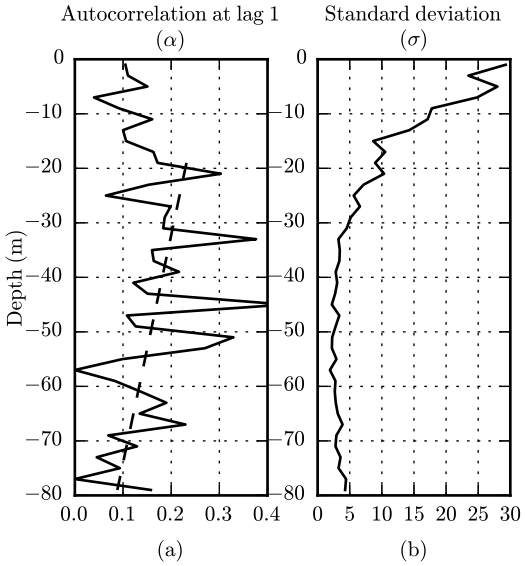

Fig. 4. AR(1) parameters for each 2 m thick layer between the surface and a depth of 80 m: (a) autocorrelation coefficient at lag 1 (α) with the regression line (dotted line) and (b) standard deviation of Gaussian noise (σ).

modeling [48].

$X(z)$ is considered as a random process in the following. Based on measured data (Fig. 1), this process cannot be considered to be stationary throughout the 80 m long profiles. Instead, we estimated $X(z)$ in 2-m thick chunks in which the random noise was assumed to be stationary. In addition, successive measurements (at 5-cm resolution) appeared to be correlated, implying that the noise must be represented by an auto-regressive process. Indeed, in an auto-regressive model of order p, an observation is regarded as being due to a linear combination of its previous p states, plus a random stochastic term (i.e., zero-mean Gaussian noise), which represents the uncorrelated forcings acting on the system [49].

To be used for statistical analysis, the irregularly-spaced density measurements were first uniformly re-sampled. To this end, a Gaussian gridding was used (see [50], [51]). The data points of the original series are convolved with a Gaussian kernel. As a result, the data points are smeared over their neighboring equi-spaced points, which are more densely distributed. This type of method produces more realistic values than simple interpolation, particularly when there are many data gaps [52]. An example of a re-sampling profile is given for the 2 m layer between a depth of 4 and 6 m in profile 1 in Fig. 3a. Profiles were re-sampled on a 3 cm regular grid, in agreement with the average layer thickness estimated in literature [12], [46].

In order to accurately estimate the parameters of the auto-regressive process, we combined all the measured profiles in each 2 m chunk. Indeed, the profiles were collected in the area where the structure snowpack was assumed to be statistically homogeneous, i.e. we assumed each measured profile is one realization of the same statistical process. Thus, auto-regressive parameters were estimated from series of about 400 measurements (from ten ice cores) near the surface and about 80 measurements (from two ice cores) below 30 m.

The partial autocorrelation functions (not shown) computed from a series suggest that a first order autoregressive model (AR(1)) is adequate. AR(1) parameters were estimated for each 2 m chunk using the "statsmodels" python toolbox [53], where the AR(1) process is defined as:

$$X_i = \alpha X_{i-1} + \epsilon \tag{8}$$

and α is the autocorrelation of series at lag 1 and ϵ is a zero-mean Gaussian noise with a standard deviation σ. The standard deviation is estimated as $\sigma^2 = \frac{1}{N}\sum_{k=1}^{N}(X_k - \bar{X} - \alpha(X_{k-1} - \bar{X}))^2$, with N the number of 3 cm layer, and k the index numbering the layers starting from the top of the 2 m chunk.

Fig. 3b, c shows the autocorrelation function calculated from a series at a depth of 4-6 m below the surface and at a depth of 72-74 m to illustrate the difference in the statistical processes with depth. Autocorrelations at lag 1, i.e. when one 3 cm layer is shifted, gives α for each layer (about 0.14 and 0.05 respectively). Fig. 4a shows α computed for each 2 m layer. α is about 0.1 near the surface and decreases to 0.05 at 80 m, meaning the correlation between 3 cm layers decreases. This may be due to densification: a layer that is 10 cm thick at the surface (i.e. corresponding to annual accumulation [54]–[56]) is only about 4.5 cm thick at a depth of 80 m. Note that variability of α is lower near the surface than below a depth of 20 m. This is probably due to the fact only two measured profiles were available to estimate α below 20 m. However, below 20 m, the α profile appears to decrease linearly with increasing depth, which is consistent with densification. In parallel, σ is maximum near the surface (about 25 kg m^{-3}) and reaches a minimum near a depth of 50 m (about 2 kg m^{-3}).

To generate density profiles down to the bedrock, α and σ were linearly extrapolated below a depth of 80 m. α was found to reach zero at about 150 m. σ is assumed to be zero below a depth of 600 m, in agreement with the pure ice region defined in Section IV-A.

$X(z)$ was generated independently for each 2 m layer using the estimated AR(1) processes to a depth of 300 m with 3 cm layers. To keep the computational resources of the emission

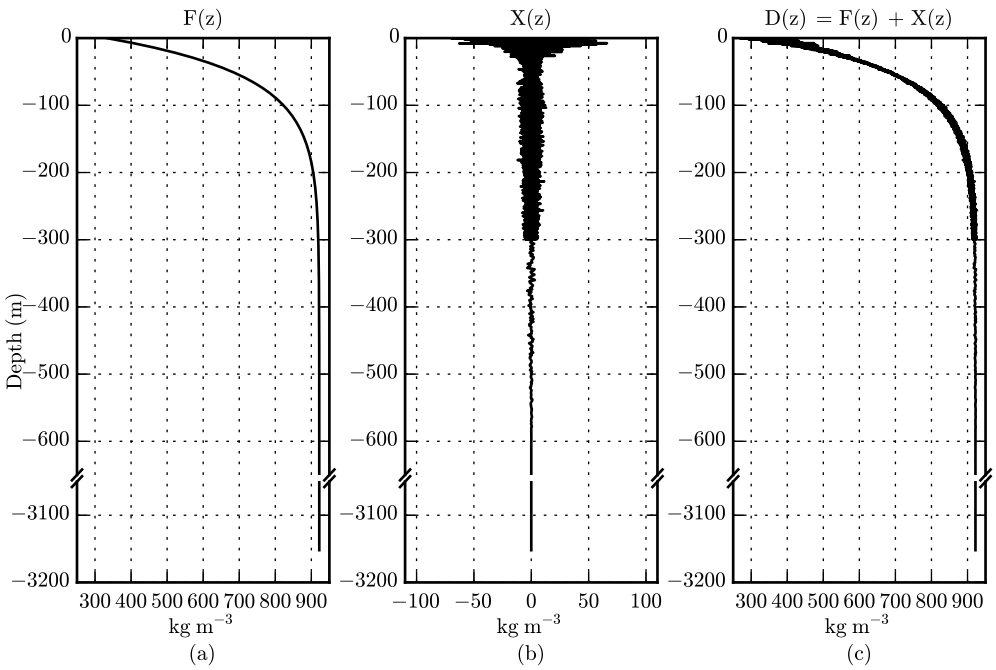

Fig. 5. Example of a generated snow density profile: (a) deterministic part $F(z)$; (b) random part $X(z)$; (c) generated density $D(z) = F(z) + X(z)$.

models realistic, we chose to limit the number of layers to a region where density variability is very low. Thus, between 300 m and 600 m, the layers are 2 m thick. $X(z)$ is a zero-mean Gaussian noise with σ standard deviation. Below 600 m, the layers are 50 m thick and the density variability $X(z)$ is equal to zero. Fig. 5b shows an example of generated $X(z)$ and Fig. 5c, the associated density profile, i.e. $F(z) + X(z)$.

The final brightness temperature was the average of all 10000 WALOMIS simulation results running with 10000 profiles generated as described in this section. The uncertainty was estimated to be about 0.2 K from 1000 final brightness temperatures. In order to perform reliable comparison, DMRT-ML final brightness temperature was computed with same method.

V. Results and Discussion

Simulations results obtained using the snow proprieties described in the previous section were compared with SMOS microwave observations. The aim was to evaluate the influence of the ice dielectric constant formulation and also to identify the most suitable electromagnetic model to simulate brightness temperature at L-band. The best configuration was then used to investigate snowpack properties at L-band.

A. Sensitivity to ice dielectric constant

Fig. 6 shows simulations performed with DMRT-ML and WALOMIS models with the two different dielectric loss formulations from Mätzler [29], ε''_{iceM} and Tiuri *et al.* [25], ε''_{iceT} (Section III-C).

Both model simulations performed with ε''_{iceM} clearly overestimated the observations. Using ε''_{iceT} considerably improved both model simulations.

This result is to be expected, because ε''_{iceT} formula is specially established from low microwave frequencies, which was not the case of ε''_{iceM}. However, the validation was performed down to -30°C whereas the temperature of the snowpack at Dome C is -55°C below a depth of 10 m and can be even lower near the surface in winter. Nevertheless, the marked improvement in the simulations suggests that ε''_{iceT} is more suitable for L-band simulation even at temperatures lower than ε''_{iceM}. In the following, Tiuri *et al.* [25] formulation is used.

B. Model comparisons

DMRT-ML did not reproduce the SMOS observations despite the improvement provided by Tiuri *et al.* [25] dielectric loss formulation. Moreover, tests of simulation with the grain size profile increased by a factor 5 (which is unrealistic for Dome C) show only a minor decrease of brightness temperatures (∼-0.5 K). This confirms that the grain size is not the cause of the DMRT-ML simulation discrepancy. In particular, the polarization ratio was significantly overestimated. This ratio decreases with the number and intensity of internal reflections within the snowpack [12], [57]. This suggests that DMRT-ML underestimates these reflections, unlike WALOMIS, which reproduced the observations at incidence angle lower than 55° quite well.

With WALOMIS, the root mean square error (RMSE) was 2.2 K, but only 1.2 K for incidence angles below 55°.

The discrepancies increased at high incidence angles with both models, and at both polarizations, the brightness temperatures were underestimated. This may be explained by the assumption of flat interfaces in both models, or the lower accuracy of SMOS observations at such large angles. Similar behavior has already been observed at higher frequencies [38].

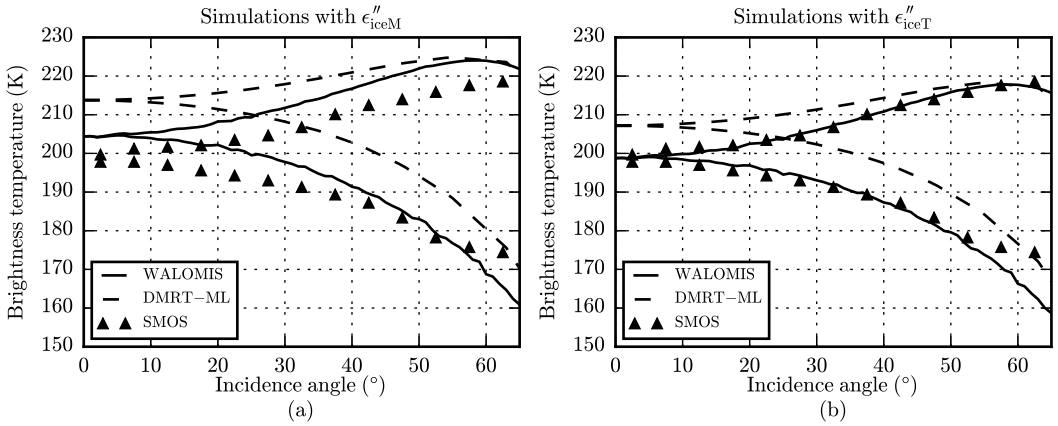

Fig. 6. Modeled brightness temperature (K) with WALOMIS (solid line) and DMRT-ML (dashed line) compared with SMOS observations (triangles) between 0° and 65° of incidence. Simulations were performed with ice dielectric loss (ε''_{ice}) from (a) Mätzler [29] and (b) Tiuri *et al.* [25].

Overall, the coherent approach is better than the RT approach because it accounts for interference effects between layers whose thickness is typically less than that of the wavelength. WALOMIS can thus be used to gain a better understanding of the L-band signal.

C. Sensitivity of L-band brightness temperature to snow properties

WALOMIS was first used to estimate the penetration of microwave radiation into the ice sheet. Second, sensitivity of L-band brightness temperature to seasonal variations in temperature was investigated. Last, the influence of the density was evaluated.

1) Emission e-folding depth: To estimate emission e-folding depth, the relative contribution of each firn layer to the total emission observed by the satellite was determined. For each layer l, a simulation was run with an increase in the temperature of 1 K in layer l only. The resulting brightness temperature, written $T_{B_l}^{+1K}$, was then compared to the brightness temperature obtained from the reference simulation performed with the original temperature profile (T_B^{ref}) as described in the previous section. The difference was normalized by the thickness of the layer yielding the normalized contribution of layer l to the total signal:

$$\Delta T_{B_l}(z) = \frac{T_{B_l}^{+1K}(z) - T_B^{ref}}{h_l} \tag{9}$$

Percent of contribution of each layer is computed from the integral of layer contribution on the whole snowpack. Sum of this contribution from the surface indicates that 50% of the signal emanates from the top 170 m, 67% from 250 m, 90% from 470 m, and 99% from 860 m (Fig. 7). Note that at Dome C, the bedrock contributes little, but its contribution could be significant in other locations where the ice sheet is not as thick. The emission e-folding depth (usually defined as the depth at which the contribution reaches 67%) is an order of magnitude higher at L-band than at C-band [58]. This is explained by both less scattering caused by snow grains and lower absorption. Since absorption is sensitive to temperature,

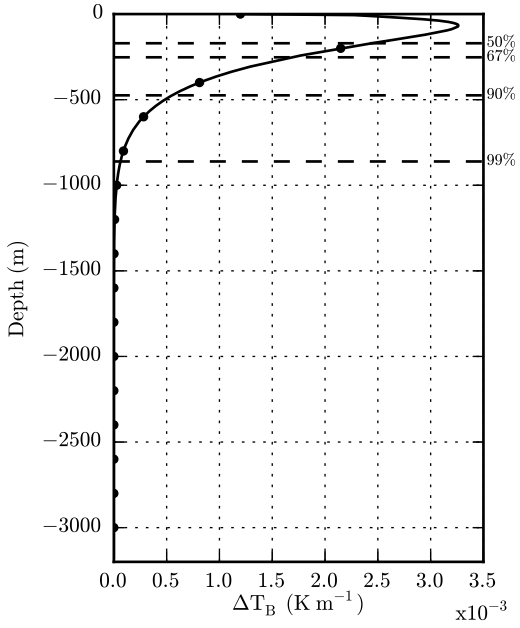

Fig. 7. Contribution of each layer to the total brightness temperature (K m^{-1}).

the emission e-folding depth in warmer regions could be lower even for a snow structure equivalent to that of Dome C. For instance, for a profile with constant temperature at -25°C, the emission e-folding depth is 106 m, more than half the actual emission e-folding depth at Dome C.

Much greater emission e-folding depths were obtained with ε''_{iceM} because of the lower dielectric loss predicted by this formulation. However, owing to the discrepancies between the models and the observations, it is unlikely that these estimations are relevant.

2) Surface temperature sensitivity: L-band observations collected by SMOS or by DOMEX ground-radiometer [59] revealed no seasonal cycle, which can be explained by the deep penetration at L-band, and the shallow penetration of the seasonal wave of temperature into the snowpack [5]. To confirm this hypothesis, we ran WALOMIS with temperature

profiles at Dome C measured in summer and winter (Fig. 1c). The temperature varied by about 35°C at the surface and only by 10°C at a depth of 2 m between the two seasons.

WALOMIS simulations showed that the mean difference was only 0.21 K at V polarization and 0.33 K at H polarization. At 0° of incidence, the difference was 0.24 K. However, at V polarization, there was a slight decrease in the difference with the increase in the angle of incidence (0.18 K at 55°) whereas it increased at H polarization (0.43 K at 55°).

This confirms that seasonal variations in surface temperature are very small [60] and are undetectable with SMOS. However, with an accuracy of 0.15 K, Aquarius should be able to detect these variations. Dome C is therefore a good site for the calibration of L-band sensors since temperature variations are routinely measured or are predictable with sufficient accuracy [5].

3) Snow density sensitivity: As explained in Section IV-B, the density profile can be decomposed into a deterministic part $F(z)$, and a random part $X(z)$. Several WALOMIS simulations were run to test sensitivity of L-band brightness temperature to these two different components of density.

Fig. 8a shows brightness temperature simulations where the deterministic profile is constant (at 400 and 700 kg m^{-3} respectively) compared to brightness temperature simulated with the deterministic part deduced from measurements (used as reference). The random part is similar in all these simulations. The mean difference was, respectively, +1 K and -3 K for deterministic part of 400 and 700 kg m^{-3} at V polarization, and -2 K and -5 K at H polarization. Thus, although the difference in the deterministic part is very large (300 kg m^{-3}), on average, it differed by less than 5 K from the reference simulation.

Two simulations were run to estimate sensitivity to density variability (Fig. 8b) where the random part was increased (resp. decreased) by a factor of two. They were compared to the reference simulation. At V polarization, the mean difference with respect to the reference simulation was -24 K with the increased variability and +7 K with the decreased variability, and at H polarization, -47 K and +16 K, respectively. On average, H polarization was twice more affected by changes in the random part than V polarization. Moreover, at H polarization, sensitivity tended to increase with an increase in the angle of incidence (e.g. up to +55 K for the stronger random part and -22 K for the weaker part at 55°) whereas, at V polarization, sensitivity tended to decrease (e.g. up to -7 K for the stronger random part and +2 K for the weaker at 55°).

To sum up, the random part of the density profiles had a stronger influence on the simulation than the deterministic part. Indeed an uncertainty of a few kg m^{-3} in the deterministic part did not alter the results of the simulation, whereas changes in the amplitude of the random part had a strong impact. This highlights the need for accurate knowledge of density variability, particularly in first hundred meters of snowpack, where is it the largest.

VI. Conclusion

In this study, two electromagnetic models driven by in situ measurements of snow properties were used to simulate the L-band microwave emission at Dome C, Antarctica. Comparisons with SMOS observations showed that the coherent model WALOMIS, based on the wave approach, is better suited to low frequencies than the incoherent model DMRT-ML, based on radiative transfer. This is mainly because in the coherent model, interference effects between layers are taken into account. However, WALOMIS does not account for scattering by snow grain size. In a next step, this model will be adapted to account for snow grain size, especially to be able to apply the coherent approach at higher frequencies than at L-band, where scattering and internal reflection contribute equally.

Two formulations of the dielectric constant of pure ice were tested. The Tiuri *et al.* [25] formula clearly yielded better results and could probably be recommended for low frequencies. However, due to lack of measurements of this constant at L-band frequencies and under cold temperatures, more work is needed to improve the results presented here, especially for the estimation of the emission e-folding depth, which is very sensitive to the dielectric loss.

The emission e-folding depth estimated with WALOMIS was about 250 m. The region that contributes 99% of the signal extends down to 900 m. This penetration is very large compared to that at higher frequencies (e.g. about 20 m at C-band), and suggests that in regions where the snowpack is less than 900 m thick, the bedrock may contribute to the emission.

The very limited sensitivity of L-band data to seasonal variations in temperature suggested in previous studies was confirmed here. With variations around 0.2 K, this is well below the SMOS radiometer noise level and close to that of Aquarius. In any case, this confirms that the Antarctic ice sheet is a good target for calibration of satellites carrying low frequency instruments.

The WALOMIS simulations revealed the strong influence of the density profiles. The random part of density plays a more important role than the deterministic part. Thus, measurements of density down to 80 m are particularly valuable because they give a realistic estimation of density variability, which is indispensable for the simulation of L-band emission.

Acknowledgment

This study benefited from strong support from the French space agency (CNES) through the SMOS TOSCA project. In situ measurements were conducted in the framework the French Polar Institute (IPEV) BIPOL project. ANR MONISNOW contributed to the experimental setting. Complementary in situ measurements were funded by INSU-CNRS programs (LEFE NIEVE and Méso Equipement Glacio Concordia) and IPEV (NIVO project). We thank F. Cabot for his help with the SMOS L1C product.

References

[1] J. Turner, T. Lachlan-Cope, S. Colwell, G. Marshall, and W. Connolley, "Significant warming of the antarctic winter troposphere," *Science*, vol. 311, no. 5769, pp. 1914–1917, 2006.

[2] S. Surdyk, "Using microwave brightness temperature to detect short-term surface air temperature changes in antarctica: An analytical approach," *Remote Sens. Environ.*, vol. 80, no. 2, pp. 256–271, 2002.

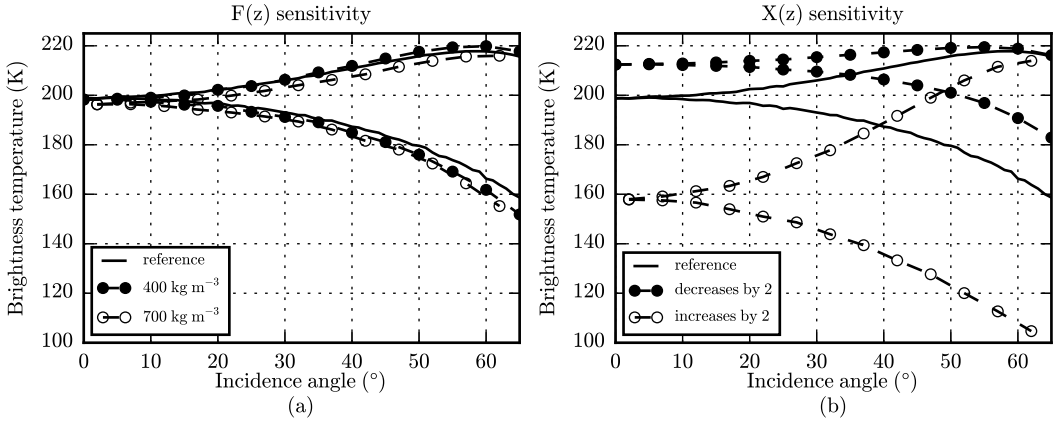

Fig. 8. Brightness temperature (K) modeled by WALOMIS with (a) the deterministic part $F(z)$ as computed with (7) (reference, solid line), equal to 400 kg m^{-3} (black circles) and to 700 kg m^{-3} (white circles); (b) the random part $X(z)$ as computed in Section IV-B (reference, solid line), increases by a factor two (black circles), and decreases by a factor two (white circles).

[3] D. P. Winebrenner, E. J. Steig, and D. P. Schneider, "Temporal covariation of surface and microwave brightness temperatures in antarctica, with implications for the observation of surface temperature variability using satellite data," *Ann. Glaciol.*, vol. 39, no. 1, pp. 346–350, 2004.

[4] C. Shuman, R. Alley, S. Anandakrishnan, and C. Stearns, "An empirical technique for estimating near-surface air temperature trends in central greenland from ssm/i brightness temperatures," *Remote Sens. Environ.*, vol. 51, no. 2, pp. 245–252, 1995.

[5] G. Picard, L. Brucker, M. Fily, H. Gallée, and G. Krinner, "Modeling time series of microwave brightness temperature in antarctica," *J. Glaciol.*, vol. 55, no. 191, pp. 537–551, 2009.

[6] Y. H. Kerr, P. Waldteufel, J.-P. Wigneron, J. Martinuzzi, J. Font, and M. Berger, "Soil moisture retrieval from space: The soil moisture and ocean salinity (smos) mission," *IEEE Trans. Geosci. Remote Sens.*, vol. 39, no. 8, pp. 1729–1735, 2001.

[7] G. Lagerloef, F. Colomb, D. Le Vine, F. Wentz, S. Yueh, C. Ruf, J. Lilly, J. Gunn, and Y. Chao, "The aquarius/sac-d mission: Designed to meet the salinity remote-sensing challenge," *Oceanography*, vol. 21, no. 1, pp. 68–81, 2008.

[8] J. T. Pulliainen, J. Grandell, and M. T. Hallikainen, "Hut snow emission model and its applicability to snow water equivalent retrieval," *IEEE Trans. Geosci. Remote Sens.*, vol. 37, no. 3, pp. 1378–1390, 1999.

[9] A. Wiesmann and C. Mätzler, "Microwave emission model of layered snowpacks," *Remote Sens. Environ.*, vol. 70, no. 3, pp. 307–316, 1999.

[10] L. Tsang, J. Pan, D. Liang, Z. Li, D. W. Cline, and Y. Tan, "Modeling active microwave remote sensing of snow using dense media radiative transfer (dmrt) theory with multiple-scattering effects," *IEEE Trans. Geosci. Remote Sens.*, vol. 45, no. 4, pp. 990–1004, 2007.

[11] S. Surdyk and M. Fily, "Results of a stratified snow emissivity model based on the wave approach: application to the antarctic ice sheet," *J. Geophys. Res.*, vol. 100, no. C5, pp. 8837–8848, 1995.

[12] R. D. West, D. P. Winebrenner, L. Tsang, and H. Rott, "Microwave emission from density-stratified antarctic firn at 6 cm wavelength," *J. Glaciol.*, vol. 42, no. 140, pp. 63–76, 1996.

[13] G. Picard, L. Brucker, A. Roy, F. Dupont, M. Fily, A. Royer, and C. Harlow, "Simulation of the microwave emission of multi-layered snowpacks using the dense media radiative transfer theory: the dmrt-ml model," *Geosci. Model Dev.*, vol. 6, no. 4, pp. 1061–1078, 2013.

[14] K. McMullan, M. A. Brown, M. Martín-Neira, W. Rits, S. Ekholm, J. Marti, and J. Lemanczyk, "Smos: The payload," *IEEE Trans. Geosci. Remote Sens.*, vol. 46, no. 3, pp. 594–605, 2008.

[15] Y. H. Kerr, P. Waldteufel, J.-P. Wigneron, S. Delwart, F. Cabot, J. Boutin, M.-J. Escorihuela, J. Font, N. Reul, C. Gruhier *et al.*, "The smos mission: New tool for monitoring key elements ofthe global water cycle," *Proc. IEEE*, vol. 98, no. 5, pp. 666–687, 2010.

[16] G. Macelloni, M. Brogioni, and R. Rahmoune, "Characterization of the spatial and temporal stability of the east-antarctic plateau in the low-microwave bands," *12th Specialist Meeting on Microwave Radiometry and Remote Sensing of the Environment (MicroRad)*, pp. 1–4, 2012.

[17] S. S. Kristensen, S. S. Søbjærg, J. E. Balling, and N. Skou, "Domecair campaign emirad data: Presentation and analysis," ESA DOMECair 2013, Tech. Rep., 2013. [Online]. Available: https://earth.esa.int/web/guest/campaigns

[18] L. Tsang and J. A. Kong, *Scattering of Electromagnetic Waves, vol.3: Advanced Topics*. Wiley Interscience, 2001.

[19] L. Brucker, G. Picard, L. Arnaud, J.-M. Barnola, M. Schneebeli, H. Brunjail, E. Lefebvre, and M. Fily, "Modeling time series of microwave brightness temperature at dome c, antarctica, using vertically resolved snow temperature and microstructure measurements," *J. Glaciol.*, vol. 57, no. 201, pp. 171–182, 2011.

[20] F. Dupont, G. Picard, A. Royer, A. Langlois, M. Fily, A. Roy, and N. Champollion, "Modeling the microwave emission of bubbly ice: Applications to blue ice and superimposed ice in the antarctic and arctic," *IEEE Trans. Geosci. Remote Sens.*, vol. 52, no. 10, pp. 6639 – 6651, 2014.

[21] S. Chandrasekhar, *Radiative transfer*. Courier Dover Publications, 1960.

[22] L. Tsang, J. A. Kong, and K.-H. Ding, *Scattering of Electromagnetic Waves, vol.1: Theories and Applications*. Wiley Interscience, 2000.

[23] C. Mätzler, "Applications of the interaction of microwaves with the natural snow cover," *Remote sens. rev.*, vol. 2, no. 2, pp. 259–387, 1987.

[24] L. Tsang, J. Kong, and R. Shin, *Theory of microwave remote sensing*. Wiley-Interscience, 1987.

[25] M. Tiuri, A. Sihvola, E. Nyfors, and M. Hallikaiken, "The complex dielectric constant of snow at microwave frequencies," *IEEE J. Ocean. Eng.*, vol. 9, no. 5, pp. 377–382, 1984.

[26] G. Hufford, "A model for the complex permittivity of ice at frequencies below 1 thz," *Int. J. Infrared Millimeter Waves*, vol. 12, no. 7, pp. 677–682, 1991.

[27] T. Matsuoka, S. Fujita, and S. Mae, "Effect of temperature on dielectric properties of ice in the range 5–39 ghz," *J. Appl. Phys.*, vol. 80, no. 10, pp. 5884–5890, 1996.

[28] J. H. Jiang and D. L. Wu, "Ice and water permittivities for millimeter and sub-millimeter remote sensing applications," *Atmospheric Science Letters*, vol. 5, no. 7, pp. 146–151, 2004.

[29] C. Mätzler, *Thermal microwave radiation: applications for remote sensing*. Institution of Engineering and Technology, 2006, vol. 52.

[30] W. Dierking, S. Linow, and W. Rack, "Toward a robust retrieval of snow accumulation over the antarctic ice sheet using satellite radar," *J. Geophys. Res.-Atmos.*, vol. 117, no. D9, 2012.

[31] A. J. Gow, "Deep core studies of the accumulation and densification of snow at byrd station and little america v, antarctica." *CRREL Research Report 197*, 1968.

[32] R. B. Alley and C. R. Bentley, "Ice-core analysis on the siple coast of west antarctica," *Ann. Glaciol.*, vol. 11, pp. 1–7, 1988.

[33] S. Kipfstuhl, S. H. Faria, N. Azuma, J. Freitag, I. Hamann, P. Kaufmann, H. Miller, K. Weiler, and F. Wilhelms, "Evidence of dynamic recrystallization in polar firn," *J. Geophys. Res.-Sol. Ea.*, vol. 114, no. B5, 2009.

[34] M. Hörhold, S. Kipfstuhl, F. Wilhelms, J. Freitag, and A. Frenzel, "The densification of layered polar firn," *J. Geophys. Res.-Ea. Surf.*, vol. 116, no. F1, 2011.

[35] L. Arnaud, G. Picard, N. Champollion, F. Domine, J. Gallet, E. Lefebvre, M. Fily, and J. Barnola, "Measurement of vertical profiles of snow

specific surface area with a 1 cm resolution using infrared reflectance: instrument description and validation," *J. Glaciol.*, vol. 57, no. 201, pp. 17–29, 2011.

[36] T. C. Grenfell and S. G. Warren, "Representation of a nonspherical ice particle by a collection of independent spheres for scattering and absorption of radiation," *J. Geophys. Res.-Atmos.*, vol. 104, no. D24, pp. 31 697–31 709, 1999.

[37] A. Roy, G. Picard, A. Royer, B. Montpetit, F. Dupont, A. Langlois, C. Derksen, and N. Champollion, "Brightness temperature simulations of the canadian seasonal snowpack driven by measurements of the snow specific surface area," *IEEE Trans. Geosci. Remote Sens.*, vol. 51, no. 9, pp. 4692–4704, 2013.

[38] G. Picard, A. Royer, L. Arnaud, and M. Fily, "Influence of meter-scale wind-formed features on the variability of the microwave brightness temperature around dome c in antarctica," *The Cryosphere*, vol. 7, no. 4, pp. 3675–3716, 2014.

[39] G. Durand, J. Weiss, V. Lipenkov, J. Barnola, G. Krinner, F. Parrenin, B. Delmonte, C. Ritz, P. Duval, R. Röthlisberger *et al.*, "Effect of impurities on grain growth in cold ice sheets," *J. Geophys. Res.-Ea. Surf.*, vol. 111, no. F1, 2006.

[40] K. Pol, V. Masson-Delmotte, S. Johnsen, M. Bigler, O. Cattani, G. Durand, S. Falourd, J. Jouzel, B. Minster, F. Parrenin, C. Ritz, H. C. Steen-Larsen, and B. Stenni, "New mis 19 epica dome c high resolution deuterium data: Hints for a problematic preservation of climate variability at sub-millennial scale in the "oldest ice"," *Earth Planet. Sci. Lett.*, vol. 298, no. 1, pp. 95–103, 2010.

[41] F. Rémy and I. E. Tabacco, "Bedrock features and ice flow near the epica ice core site (dome c, antarctica)," *Geophys. Res. Lett.*, vol. 27, no. 3, pp. 405–408, 2000.

[42] K. J. Ueltzhoffer, V. Bendel, J. Freitag, S. Kipfstuhl, D. Wagenbach, S. H. Faria, and C. S. Garbe, "Distribution of air bubbles in the edml and edc (antarctica) ice cores, using a new method of automatic image analysis," *J. Glaciol.*, vol. 56, no. 196, pp. 339–348, 2010.

[43] V. Bendel, K. J. Ueltzhöffer, J. Freitag, S. Kipfstuhl, W. F. Kuhs, C. S. Garbe, and S. H. Faria, "High-resolution variations in size, number and arrangement of air bubbles in the epica dml (antarctica) ice core," *J. Glaciol.*, vol. 59, no. 217, pp. 972–980, 2013.

[44] V. Y. Lipenkov, A. Salamatin, and P. Duval, "Bubbly-ice densification in ice sheets: Ii. applications," *J. Glaciol.*, vol. 43, no. 145, pp. 397–407, 1997.

[45] H. Narita, N. Azuma, T. Hondoh, M. Fujii, M. Kawaguchi, S. Mae, H. Shoji, T. Kameda, and O. Watanabe, "Characteristics of air bubbles and hydrates in the dome fuji ice core, antarctica," *Ann. Glaciol.*, vol. 29, no. 1, pp. 207–210, 1999.

[46] T. Hondoh, H. Narita, A. Hori, M. Fujii, H. Shoji, T. Kameda, S. Mae, S. Fujita, T. Ikeda, H. Fukasawa *et al.*, "Basic analyses of dome fuji deep ice core part 2: physical properties," *Polar meteorology and glaciology*, vol. 13, pp. 90–98, 1999.

[47] A. W. Bingham and M. R. Drinkwater, "Recent changes in the microwave scattering properties of the antarctic ice sheet," *IEEE Trans. Geosci. Remote Sens.*, vol. 38, no. 4, pp. 1810–1820, 2000.

[48] L. Arnaud, J. M. Barnola, and P. Duval, "Physical modeling of the densification of snow/firn and ice in the upper part of polar ice sheets," *Physics of ice core records*, pp. 285–305, 2000.

[49] H. von Storch and F. W. Zwiers, *Statistical analysis in climate research*. Cambridge University Press, 2001.

[50] L. Greengard and J.-Y. Lee, "Accelerating the nonuniform fast fourier transform," *SIAM review*, vol. 46, no. 3, pp. 443–454, 2004.

[51] A. Dutt and V. Rokhlin, "Fast fourier transforms for nonequispaced data," *SIAM Journal on Scientific computing*, vol. 14, no. 6, pp. 1368–1393, 1993.

[52] H. Schomberg and J. Timmer, "The gridding method for image reconstruction by fourier transformation," *IEEE Trans. Med. Imag.*, vol. 14, no. 3, pp. 596–607, 1995.

[53] W. McKinney, J. Perktold, and S. Seabold, "Time series analysis in python with statsmodels," *Proceedings of the 10th Python in Science Conference*, pp. 96–102, 2011.

[54] J. Petit, J. Jouzel, M. Pourchet, and L. Merlivat, "A detailed study of snow accumulation and stable isotope content in dome c (antarctica)," *J. Geophys. Res.-Oc.*, vol. 87, no. C6, pp. 4301–4308, 1982.

[55] M. Frezzotti, M. Pourchet, O. Flora, S. Gandolfi, M. Gay, S. Urbini, C. Vincent, S. Becagli, R. Gragnani, M. Proposito *et al.*, "Spatial and temporal variability of snow accumulation in east antarctica from traverse data," *J. Glaciol.*, vol. 51, no. 172, pp. 113–124, 2005.

[56] F. Parrenin, G. Dreyfus, G. Durand, S. Fujita, O. Gagliardini, F. Gillet, J. Jouzel, K. Kawamura, N. Lhomme, V. Masson-Delmotte *et al.*, "Ice flow modelling at epica dome c and dome fuji, east antarctica," *Clim. Past*, vol. 3, no. 1, pp. 243–259, 2007.

[57] N. Champollion, G. Picard, L. Arnaud, E. Lefebvre, and M. Fily, "Hoar crystal development and disappearance at dome c, antarctica: observation by near-infrared photography and passive microwave satellite," *The Cryosphere*, vol. 7, pp. 1247–1262, 2013.

[58] G. Macelloni, M. Brogioni, P. Pampaloni, and A. Cagnati, "Multifrequency microwave emission fromthe dome-c area on the east antarctic plateau: Temporal and spatial variability," *IEEE Trans. Geosci. Remote Sens.*, vol. 45, no. 7, pp. 2029–2039, 2007.

[59] G. Macelloni, M. Brogioni, P. Pampaloni, A. Cagnati, and M. R. Drinkwater, "Domex 2004: An experimental campaign at dome-c antarctica for the calibration of spaceborne low-frequency microwave radiometers," *IEEE Trans. Geosci. Remote Sens.*, vol. 44, no. 10, pp. 2642–2653, 2006.

[60] M. R. Drinkwater, N. Floury, and M. Tedesco, "L-band ice-sheet brightness temperatures at dome c, antarctica: spectral emission modelling, temporal stability and impact of the ionosphere," *Ann. Glaciol.*, vol. 39, no. 1, pp. 391–396, 2004.

Marion Leduc–Leballeur received the M.Sc. degree in remote sensing from University Pierre and Marie Curie (UPMC), Paris, France, in 2008, and the Ph.D. degree in atmospheric physics conducted at the Laboratoire Atmosphères, Milieux, Observations Spatiales (LATMOS/IPSL), Paris, France, from UPMC, Paris, France, in 2012.

She joined the Laboratoire de Glaciologie et Géophysique de l'Environnement (LGGE) in 2012. Her research investigates snow properties from microwave remote sensing, using electromagnetic modeling, satellite observations and in situ measurements.

Ghislain Picard received the M.Sc. degree in remote sensing from the university of Paris VII, Paris, France, in 1997. He conducted his Ph.D. work between 1999 and 2002 at the Centre d'Etudes Spatiale de la Biosphère, Toulouse, France, where he developed several models of vegetation backscatter in the microwave range.

After a postdoctorat a the Centre of Terrestrial Carbon Dynamics at the University of Sheffield, he joined the Laboratoire de Glaciologie in Grenoble in 2005. Since then, his research has focused on the evolution of the Antarctic climate through the study of the snow, both using a variety of remote sensing techniques and field experimentation. He is involved in the development of innovative instruments for the characterization of snow physical properties.

Arnaud Mialon received the M.Sc. degree in climate and physics-chemistry of the atmosphere from Université Joseph Fourier (Grenoble, France) in 2002, and a Ph.D. degree in ocean-atmosphere hydrology from University Joseph Fourier (Grenoble, France) and in remote sensing from the University of Sherbrooke (Québec, Canada) in 2005.

He joined the Centre d'Etudes Spatiales de la Biosphère, Toulouse, France, in 2006. His fields of interest are focused on passive microwave remote sensing of continental surfaces. He is involved in the SMOS (Soil Moisture and Ocean Salinity) mission as well as in field campaigns to measure surface soil moisture.

Laurent Arnaud received the Engineering degree from the Institut National des Sciences Appliquées de Lyon in physics and materials science in 1993, and the Ph.D. degree in geophysics/geosciences from University Joseph Fourier, Grenoble in 1997.

He is a Research Engineer with the Centre National de la Recherche Scientifique (CNRS) since 2000. He has been with the Laboratoire de Spectrométrie Ionique et Moléculaire from 2000 to 2005 in charge of new developments on high resolution time of flight mass spectrometers and TEM analysis of metallic cluster landed on surfaces. Since 2006, he has been with the Laboratoire de Glaciologie et Géophysique de l'Environnement and his current research interests concern the snow and firn cover: temporal and spatial variations. His work is mainly focus on development of new instruments and remote station engineering to characterize physical and mechanical properties of polar snow and firn.

Eric Lefebvre is electronic engineer. He worked in the Laboratoire de Glaciologie et Géophysique de l'Environnement (LGGE) since 1984.

He is a specialist of embedded electronic dedicated to measurements in very cold and harsh environment in Antarctica. He has a broad experience in polar missions and participate at more than 20 summer seasons in Antarctica for field measurements.

Philippe Possenti

Yann Kerr (M '88, SM '01, F'13) received the engineering degree from Ecole Nationale Supérieure de l'Aéronautique et de l'Espace, the M.Sc. degree in electronics and electrical engineering from Glasgow University, Glasgow, Scotland, UK, and the Ph.D. degree in Astrophysique Gophysique et Techniques Spatiales, Université Paul Sabatier, Toulouse, France. His fields of interest are in the theory and techniques for microwave and thermal infrared remote sensing of the Earth, with emphasis on hydrology, water resources management. He is currently the Director of Centre d'Etudes Spatiales de la BIOsphère, Toulouse, France.

He was an EOS principal investigator (interdisciplinary investigations), and PI and precursor of the use of the SCAT over land. In 1988 he started to work on the interferometric concept applied to passive microwave earth observation and was subsequently the science lead on the MIRAS project for ESA. In 1997 he proposed the SMOS Mission, the natural outcome of the previous MIRAS work. He is currently involved in the exploitation of SMOS data, in the Cal Val activities and related level 2 soil moisture and level 3 and 4 developments. He is also working on the SMOS next concept and involved in both the Aquarius and SMAP missions. He received the World Meteorological Organization 1st prize (Norbert Gerbier), the USDA Secretary's team award for excellence (Salsa Program), the GRSS certificate of recognition for leadership in development of the first synthetic aperture microwave radiometer in space and success of the SMOS mission, and is a Distinguished Lecturer for GRSS.